Rare Metal Materials and Engineering
Volume 47, Issue 8, August 2018
Online English edition of the Chinese language journal

Available online at www.sciencedirect.com
ScienceDirect

Cite this article as: Rare Metal Materials and Engineering, 2018, 47(8): 2371-2380.

ARTICLE

Strontium-doped Hydroxyapatite Coatings Deposited on Mg-4Zn Alloy: Physical-chemical Properties and in vitro Cell Response

Shi Wei[1], Zhao Dapeng[1], Shang Peng[2], Nie Hemin[1], Zhang Yuan[1], Tang Jincheng[1]

[1] Hunan University, Changsha 410082, China; [2] Shenzhen Institutes of Advanced Technology, Chinese Academy of Sciences, Shenzhen 518055, China

Abstract: Biodegradable magnesium (Mg)-based biomaterials have draw extensively attention, due to the high strength-to-weight ratio, low elastic modulus and good biocompatibility. However, the high corrosion rate is still a major obstacle for the potential clinical applications. Therefore, the highly biocompatible hydroxyapatite (HA) coatings are usually introduced to restrain the interactions between Mg-based substrate and the body fluid environment. In the present paper, HA and strontium (Sr)-doped HA coatings were prepared on Mg-4Zn substrates by electrochemical deposition. The surface properties of the samples were characterized by scanning electron microscopy (SEM), energy dispersive spectroscopy (EDS), transmission electron microscopy (TEM), three-dimensional laser scanning microscopy (3D LSM) and a contact angle video system. The dynamic ion release, protein adsorption, cell adhesion, proliferation and differentiation behavior of the samples were also evaluated. The results reveal that the incorporation of Sr in the HA coatings leads to lattice distortion and decreased crystallinity. The smaller amount of Mg ion release of the Sr-doped HA coated samples suggests a better corrosion resistance. The improved protein adsorption and initial adhesion of mesenchymal stem cells (MSCs) of the Sr-doped samples should be due to their higher surface roughness and wettability. The introduction of Sr leads to comparable cell proliferation behavior, but significantly improved osteogenic differentiation. It is concluded that the Sr-doped HA coatings are promising candidates for the protective biocompatible coating on Mg-based implants.

Key words: strontium-doped hydroxyapatite; Mg-4Zn alloy; dynamic ion release; cell viability; osteogenic differentiation

Compared to the traditional metallic biomaterials, such as stainless steel, cobalt-chromium (CoCr) alloys and titanium (Ti) alloys, the density and Young's modulus of magnesium (Mg) alloys are more close to those of bones[1]. More importantly, the biodegradable property of Mg alloys is highly desired for bone repairing because they can degrade in vivo and thus avoid chronic inflammation reaction and secondary injury during implant removal[2]. However, the clinical applications of Mg alloys are still challenged with the rapid corrosion rate, which usually leads to local increase of alkalinity near the implant site and thus retards the healing process[3].

In order to improve the corrosion resistance and biocompatibility of Mg alloys, two approaches are generally employed. On the one hand, the alloying of Mg by adding selected non-toxic or low-toxic elements, such as yttrium (Y), zirconium (Zr) and neodymium (Nd), can lead to lower corrosion rate[4]. Zhu et al.[5] stated that zinc (Zn) is an essential trace element in the human body, and plays an important role in bone growth and the maintenance of various cellular functions. Besides, the addition of Zn into Mg leads to significantly decreased mass loss and lower volume of released hydrogen in minimum essential medium (MEM) and simulated body fluid (SBF) than commercially pure Mg (CP-Mg)[6]. On the other hand, the surface treatment or deposition of a

Received date: June 25, 2018
Foundation item: National Natural Science Foundation of China (51604104); Development and Reform Commission of Shenzhen Municipality (JCYJ20140417113430610)
Corresponding authors: Zhao Dapeng, Ph. D., College of Biology, Hunan University, Changsha 410082, P. R. China, Tel: 0086-731-88822606, E-mail: dpzhao@hnu.edu.cn

biocompatible coatings are usually applied to build a barrier between the Mg-based substrates and the biological environment[7]. The hydroxyapatite (HA) layers are of special interest, because of their high chemical and structural similarities to the mineral component of bones and teeth[8]. Wen et al.[9] reported that the HA coating on AZ31 alloy substrate significantly increases the corrosion potential. Besides, the HA coatings are ideal delivery platform for many trace elements, such as Zn and silver (Ag), by substituting Ca ions in the HA lattice[10]. Strontium (Sr) is a trace metal in human bones, and can induce opposite effects on bone resorption and formation, i.e., it stimulates the differentiation of osteoblastic cells, but inhibits the activity and differentiation of osteoclasts[1] . So Sr is also doped into HA coatings to improve bone healing and strength[12]. Xue et al.[13] prepared the Sr-containing HA coatings on Ti-6Al-4V alloy, and the presence of Sr significantly enhances the osteogenic differentiation and mineralization.

In the present investigation, Sr-doped HA coatings were deposited on Mg-4Zn alloy, and the HA coated Mg-4Zn and bare Mg-4Zn alloy were also prepared as references. The aim is to evaluate the influence of the Sr-incorporation in the HA coatings on the surface composition, structure, phase constitution, dynamic corrosion behavior and cell responses of the samples.

1 Experiment

1.1 Materials preparation

The Mg-4Zn raw material sheets were obtained from College of Materials Science and Engineering, Hunan University, and details of the processing are shown in Ref.[14]. The as-received materials were wire-electrode cut into plates with the dimension of 10 mm×10 mm×2 mm, and then ground with 600#, 1000# and 2000# grit SiC paper. The ground plates were ultrasonically cleaned in ethanol, immersed into 100 g/L NaOH solution at 90 °C for 10 min, and then washed by 180 g/L CrO_3 solution for 5 min to remove oil and surface oxide. Afterwards, the Mg-4Zn samples were ultrasonically cleaned in deionized water for 10 min and dried at 60 °C.

A series of Sr-doped HA coatings with Sr/(Ca+Sr) atomic ratios of 0%, 5% and 10% (named as 0SrHA, 5SrHA and 10SrHA) were deposited on the Mg-4Zn by electrochemical deposition. Briefly, analytical grade (AR) $CaCl_2$, $SrCl_2·6H_2O$ and $NH_4H_2PO_4$ were dissolved into deionized water with magnetic stirring at 85 °C. The coated plates with Sr/(Ca+Sr) atomic ratios of 0%, 5% and 10% are referred to as 0SrHA@Mg-4Zn, 5SrHA@Mg-4Zn and 10SrHA@Mg-4Zn, respectively.

All samples were sterilized by autoclaving prior to biomedical tests.

1.2 Surface characterization

Scanning electron microscopy (SEM, JSM-6700F, JEOL, Japan), energy dispersive spectroscopy (EDS, Inca, OXFORD, UK) in the SEM, transmission electron microscopy (TEM, JSM-2100F, JEOL, Japan) and three-dimensional Laser Scanning Microscope (3D SLM, VK-X260K, Keyence, Japan) were applied for the surface morphology, composition, phase characterization and topographical analyses, respectively.

The wettability studies were performed by a contact angle video system DSA 100, Krüss, Germany. An equal volume of distilled water (5 μL) was placed on the surface of the samples using a microsyringe. The static water contact angle was measured for 10 s after the water droplet was deposited on the membrane surface, and the measurements were done at least three times.

1.3 Ion release

The samples were placed into 10 mL SBF (Jisskang, China) solution (pH=7.4) at 37 °C for one week. At specific time points, 5 mL solution was taken and stored in centrifuge tubes prior to analysis by Inductively Coupled Plasma Atomic Emission Spectrometer (ICP-AES, PS-6, Baird, USA). 5 mL of fresh SBF solution was added to keep a constant volume of solution.

1.4 Protein adsorption

In this study, bovine serum albumin (BSA), fraction V (Sigma, purity of 99.8%) was used as the model protein, and phosphate buffer solution (PBS, K_2HPO_4/KH_2PO_4, 100 mmol/L, pH=7.4) was used for the protein solution preparation. The specimens were incubated into 1 mg/mL protein solution and maintained in a sterile humidified incubator at 37 °C for 2 h. Afterwards, PBS was used to remove the unbound proteins by washing the samples for 3 times. The proteins adsorbed on the samples were eluted after 1 h incubation at 37 °C (n=3) by 2% sodium dodecyl sulfate (SDS) and determined by a protein assay kit (Pierce, BCA Protein Assay Kit, Rockford, Illinois, USA).

1.5 Cell isolation and culture

Rat bone mesenchymal stem cells (MSCs) were isolated from the bone shaft of the femora of 4 week-old rats, and primarily cultured using the method described by Maegawa et al.[15]. The cells were obtained from at least two rats and pooled, and then seeded in a 25 cm^2 tissue culture flask with the Dulbecco's Modified Eagle Medium (DMEM) containing 10% fetal bovine serum (FBS) and antibiotics (100 U/mL penicillin G, 100 mg/mL streptomycin sulphate and 0.25 mg/mL amphotericin B) and maintained in a humidified atmosphere containing 95% air and 5% CO_2 at 37 °C. The medium in primary cultures was renewed every 2 d. At 80% confluence, the rat MSCs were harvested with trypsin/EDTA, and used for the following experiments.

1.6 Initial cell adhesion

The initial cell adhesion was evaluated by fluorescence microscopy (Nikon SMZ 1000, Japan). The MSCs were seeded onto the samples in 24-well plates at a density of $1×10^4$ cells/sample. After incubation for 2 h and 8 h, non-adhered cells were removed by rinsing with PBS. Thereafter, the attached

cells on the samples were stained with calcein, followed by imaging. Cell number was obtained from five random fields.

1.7 Cell proliferation

Extraction mediums were prepared by incubating the four configurations in DMEM supplemented with 10% FBS at 37 °C for 72 h, according to ISO 10993:5 and 10993:12. The mass to volume ratio of the samples to medium was 0.1 g/mL. The extraction mediums were sterile filtered with a 0.22 μm syringe filter for cellular experiments.

The MSCs were planted into 96-well plate at 1×10^4 cells per 100 μL of a DMEM containing 10% FBS and 1% PS in each well. The medium in each well was replaced with the 100 μL of extraction medium and again cultured for 24 h and 72 h. The cell viability was assessed by Methyl thiazolyl tetrazolium (MTT) assay, which was taken up by active cells and reduced in the mitochondria to insoluble purple formazan granules. Then the 25 μL of MTT solution was added into each well and incubated for 4 h. Next, the medium was discarded and 100 μL dimethyl sulfoxide (DMSO) was taken into each well, shaken for 10 min. Optical density (OD) of solution with cells was measured using a microplate spectrophotometer (EnSpire 2300) at a wavelength of 490 nm. Each test was repeated five times (n=5). The MSCs incubated in regular cell culture medium were used as control groups.

1.8 Osteogenic differentiation

Alkaline phosphatase (ALP) and Alizarin red S (ARS) staining were applied for osteogenic differentiation assay. MSCs at a density of 5×10^4 cells/well were seeded into the 48-well plates filled with extraction mediums. Following incubation for 7 d, MSCs were rinsed three times with PBS, fixed in 4% PFA for 30 min and stained using an ALP kit. ARS was performed after 14 d of incubation. MSCs were rinsed three times with PBS, fixed in 4% PFA for 30 min and stained using an ARS solution.

1.9 Statistical analysis

SigmaStat package (Systat software GmbH, Erkrath, Germany) was used for statistics analysis. Standard analysis comparing more than two treatments was done by the one-way ANOVA (analysis of variance). Depending on the data distribution either a one-way ANOVA or an ANOVA on ranks was performed. Post-hoc tests were Holm-Sidak or Dunn's versus the control group. Statistical values were indicated in the relevant experiments. A p<0.05 was considered statistically significant.

2 Results

2.1 Surface characterization

Fig.1 presents the surface morphologies of Mg-4Zn, 0SrHA@Mg-4Zn, 5SrHA@Mg-4Zn and 10SrHA@Mg-4Zn. Only some scratches are observed on the bare Mg-4Zn alloy, showing typical ground surface. The coated samples show the morphologies like chrysanthemum flowers aggregated on the surface of substrates. The flower-like structure on 0SrHA@Mg-4Zn samples mainly consists of loosely packed large crystal flakes and fine needle-like structures dispersed among them as shown in Fig.1b. Different from the 0SrHA@Mg-4Zn samples, the crystal flakes on the 5SrHA@Mg-4Zn and 10SrHA@Mg-4Zn samples are much smaller in size, leading to more dense-packed surfaces. Besides, more needle-like structures are observed on the latter two samples.

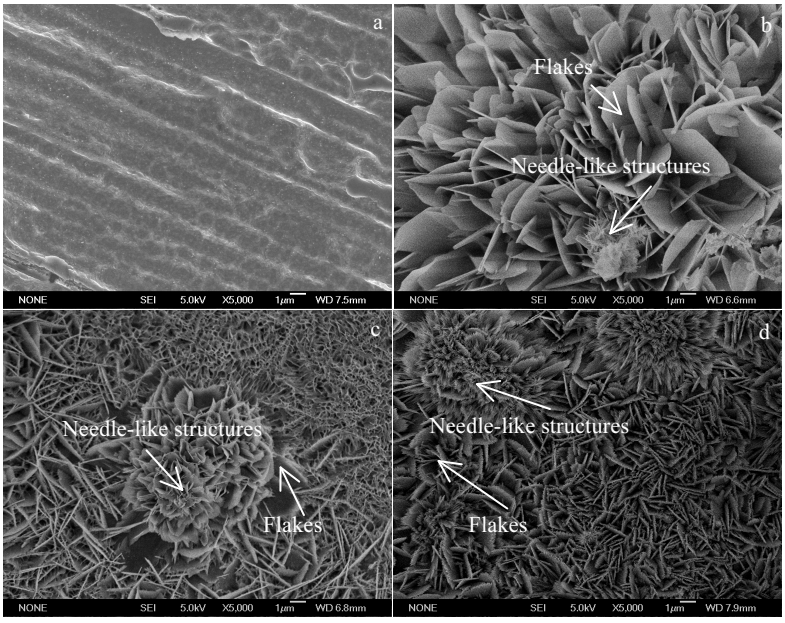

Fig.1 SEM micrographs of the surfaces: (a) as-prepared bare Mg-4Zn, (b) 0SrHA@Mg-4Zn, (c) 5SrHA@Mg-4Zn, and (d) 10SrHA@Mg-4Zn

EDS results of the surfaces of three coated groups are presented in Table 1. It is revealed that the coatings on the three samples consist of Ca-P-rich or Ca-Sr-P-rich compounds, and trace amounts of Mg and Zn should be attributed to the Mg-4Zn substrates. The 5SrHA@Mg-4Zn and 10SrHA@Mg-4Zn samples show Sr/(Ca+Sr) ratios of 4.2 at% and 9.1 at%, respectively, which are slightly lower than the designed compositions. The (Ca+Sr)/P ratios of the coatings on 0SrHA@Mg-4Zn, 5SrHA@Mg-4Zn and 10SrHA@Mg-4Zn samples are 1.34, 1.32 and 1.29, respectively.

In order to better understand the structure and phase constitutions of the three coatings, the different coatings were removed from the samples and then characterized by TEM bright field imaging and selected area electron diffraction (SAED) in the TEM as displayed in Fig.2. Generally speaking, the bright field images as presented in Fig.2a, 2b and 2c reveal that the 0SrHA, 5SrHA and 10SrHA coatings are all composed of crystal flakes with the size of 20~100 nm, and no significant differences in size distribution are observed. Besides, the crystal morphology does not show considerable change after the addition of Sr into the coating. The SAED patterns of the three coatings show typical spotty ring patterns as presented in Fig.2d. The presence of bright (002) and (211) planes as well as the dark (102) plan in the three configurations confirms the structure as close-packed hexagonal, indicating that the coatings are mainly composed of HA phase. The interplanar distance d_{002} of 0SrHA is 0.340 nm, while those of 5SrHA and 10SrHA are 0.343 and 0.345 nm, respectively. It is important to note that with increasing Sr content in the HA coatings, the diffraction rings become dim, indicating the decrease of crystallinity in the Sr-incorporated HA coatings.

In order to obtain more information about the material surfaces, the 3D LSM images were used for the topographical surface examination and roughness measurements as shown in Fig.3 and Table 2, respectively. The Mg-4Zn alloy shows different surface structures compared with the other three samples. As shown in Fig.3a and Table 2, the bare Mg-4Zn presents a relatively smooth surface with the lowest average surface roughness (R_a) and average maximum height of the profile (R_z). The 10SrHA@Mg-4Zn exhibits more peaks than other samples, and its R_a and R_z are also the highest. Although the maximum peak height of the 5SrHA@Mg-4Zn (19.7 μm) is lower than that of the 0SrHA@Mg-4Zn (45.4 μm), the two groups show comparable surface roughness.

The apparent contact angles measurements were performed in Fig.4. All the samples show hydrophilic surfaces, since all contact angles are lower than 90°. The bare Mg-4Zn alloy exhibits a significantly higher contact angle than the others. With increasing Sr content in the coating, the surface tends to

Table 1 EDS results of the surfaces of 0SrHA@Mg-4Zn, 5SrHA@Mg-4Zn and 10SrHA@Mg-4Zn samples (at%)

Samples	Ca	Sr	P	Mg	Zn	O	C
0SrHA@Mg-4Zn	17.07	-	12.74	2.91	0.11	55.71	11.46
5SrHA@Mg-4Zn	14.51	0.64	11.48	1.79	0.21	53.53	17.84
10SrHA@Mg-4Zn	12.53	1.25	10.68	2.99	0.30	51.84	20.42

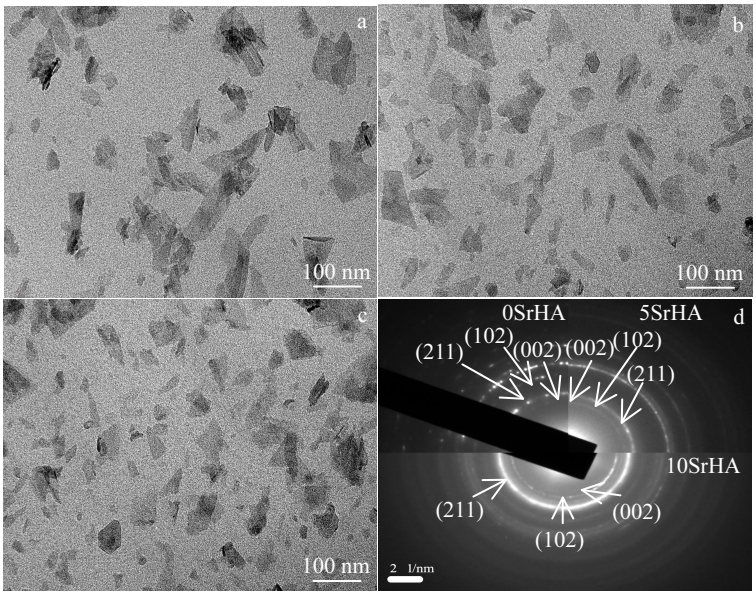

Fig.2 TEM images of the 0SrHA (a), 5SrHA (b) and 10SrHA (c) coatings, and the corresponding SAED patterns (d)

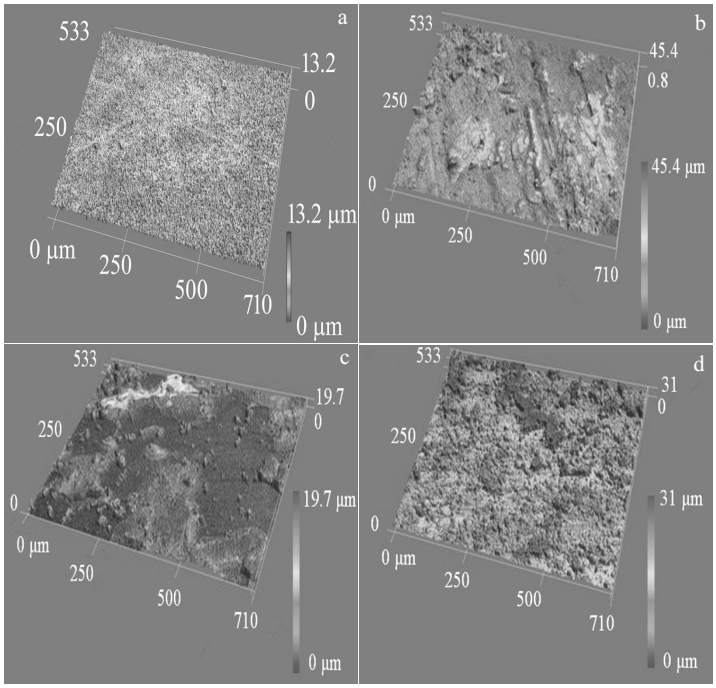

Fig.3 Surface topographic 3D views of an area of 710 μm×530 μm: (a) Mg-4Zn, (b) 0SrHA@Mg-4Zn, (c) 5SrHA@Mg-4Zn, and (d) 10SrHA@Mg-4Zn (the color scale of each profile represents the height of peaks on the surface)

Table 2 Roughness parameters on studied surfaces (μm)

	Mg-4Zn	0SrHA@Mg-4Zn	5SrHA@Mg-4Zn	10SrHA@Mg-4Zn
R_a	0.077	1.636	1.593	3.486
R_z	2.636	10.091	9.864	16.722

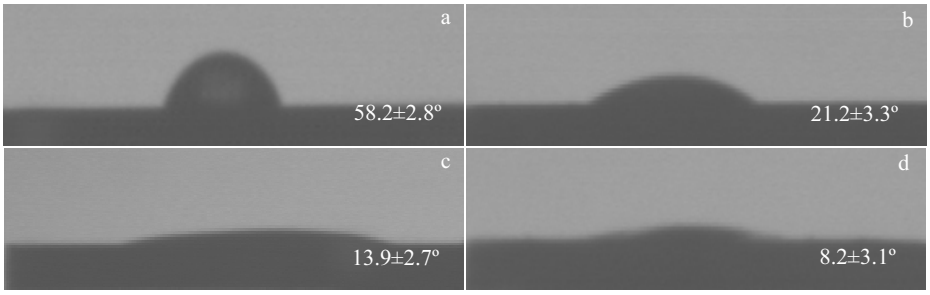

Fig.4 Initial static water contact angles and droplet images of: (a) Mg-4Zn, (b) 0SrHA@Mg-4Zn, (c) 5SrHA@Mg-4Zn, and (d) 10SrHA@Mg-4Zn

be more wettable. The contact angle of 10SrHA@Mg-4Zn samples is around 10°, indicating that the surface is almost superhydrophilic.

2.2 Ion release property

Fig.5 presents the cumulative Mg^{2+}, Ca^{2+}, Sr^{2+} and PO_4^{3-} ion release from Mg-4Zn, 0SrHA@Mg-4Zn, 5SrHA@Mg-4Zn and 10SrHA@Mg-4Zn samples into the SBF solution as a function of time. The Mg-4Zn samples show the highest amount of Mg^{2+} release and the 10SrHA@Mg-4Zn samples show the lowest (see Fig.5a). Besides, it can be observed that the concentration of Mg^{2+} tends to increase with the immersion time in the first 3 d and then gradually acheive stable values for all the three coatings. The three coated configurations present similar Ca^{2+} as well as PO_4^{3-} evolution behavior without significant difference among

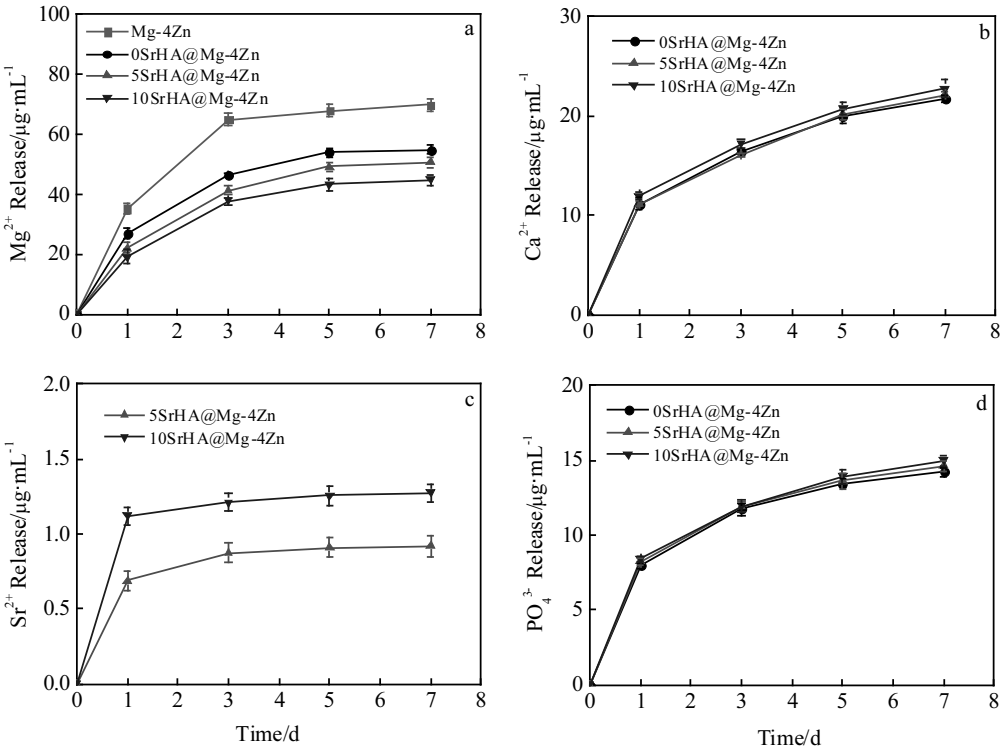

Fig.5 Ions release of Mg^{2+} (a), Ca^{2+} (b), Sr^{2+} (c) and PO_4^{3-} (d) from Mg-4Zn, 0SrHA@Mg-4Zn, 5SrHA@Mg-4Zn and 10SrHA@Mg-4Zn samples in SBF

the groups, and the concentration of Sr^{2+} released from the 10SrHA@Mg-4Zn samples is about twice as much as that of the 5SrHA@Mg-4Zn specimens as shown in Fig. 5b, 5c and 5d.

2.3 Protein adsorption

The amount of BSA adsorption on the various samples is presented in Fig.6. In general, the protein adsorption on the bare Mg-4Zn alloy is significantly lower than that of the coated samples, and the 10SrHA@Mg-4Zn exhitibts the highest amount of BSA adsoption among the coated ones. While, the adsorption on the 0SrHA@Mg-4Zn and 5SrHA@Mg-4Zn samples does not show a considerable difference.

2.4 Initial cell adhesion

The cell number of MSCs adhered on the samples for 2 h and 8 h was evaluated by fluorescence microscopy as shown in Fig.7a, and the statistical analyses are presented in Fig.7b. With increasing adhesion time, more cells adhered on the same sample configuration are observed. For the same adhesion time, the bare Mg-4Zn alloy shows significantly lower adhered cell numbers than the coated ones. After incubation for 2 h, the number of cells adhered on the three coated samples does not exhibit great disparities, but a significantly enhanced adhesion of MSCs can be observed on the samples with higher Sr-incorporated coating after cell adhesion for 8 h.

2.5 Cell proliferation

Fig.8 presents the proliferation of MSCs incubated in the Mg-4Zn, 0SrHA@Mg-4Zn, 5SrHA@Mg-4Zn and 10SrHA@Mg-4Zn extraction mediums and the regular cell culture medium (control groups) for 24 h and 72 h, and the average cell viability of the control group for 24 h was set as 100%. Fig.8b shows the statistical analyses between every two configurations. The cell proliferation significantly increases with increasing incubation time in all extracts. As for the same incubation time, the extracts of the three coated

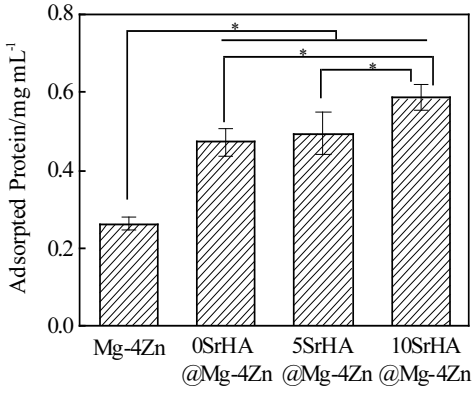

Fig.6 Protein adsorption on the various samples after incubation for 2 h in PBS containing 1 mg/mL BSA (statistically significant difference, $*P < 0.05$)

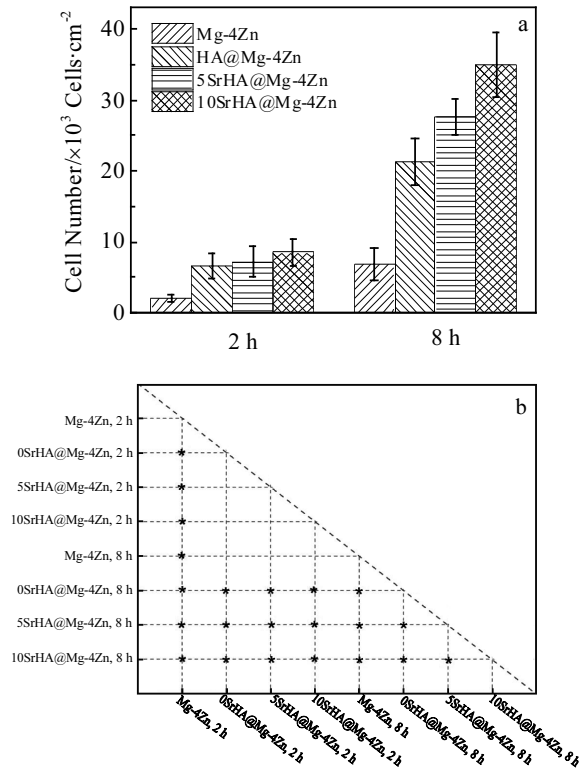

Fig. 7 Cell counting using calcein staining after adhesion on different samples for 2 h and 8 h (a); cell adhesion statistical analyses (b) (statistically significant difference between two groups, $*P < 0.05$)

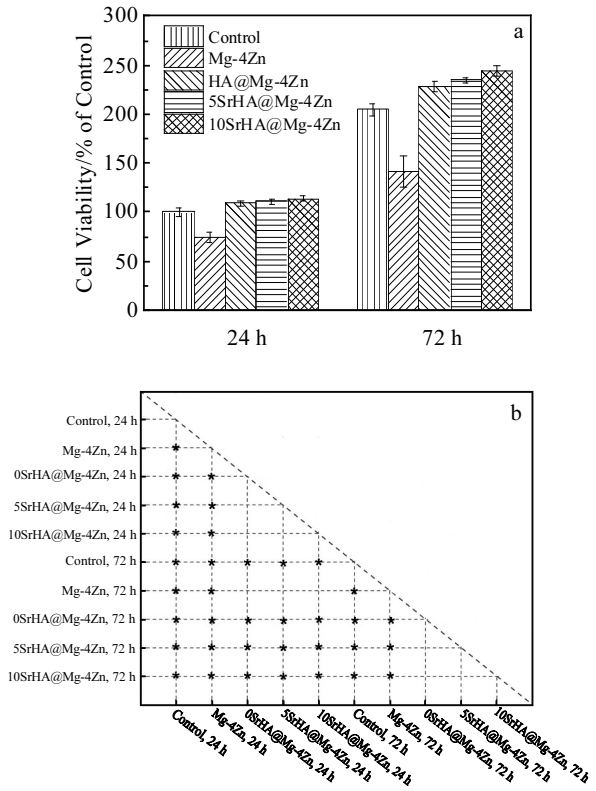

Fig. 8 MSCs proliferation in the extracts of different samples after 24 h and 72 h of culture, and the average cell viability in regular cell culture medium incubated for 24 h is set as 100% (a); cell proliferation statistical analyses (b) (statistically significant difference between two groups, $*P < 0.05$)

groups exhibit significantly improved cell proliferation compared to the control group, while, that of the Mg-4Zn group shows much lower cell viability than the control group. Besides, there are no significant differences among the cell proliferation in the 0SrHA@Mg-4Zn, 5SrHA@Mg-4Zn and 10SrHA@Mg-4Zn extraction mediums after incubation for 24 h or 72 h.

2.6 Cell differentiation

Fig.9 shows the ALP and ARS staining of MSCs after incubation in the cell culture medium as control and the different extraction mediums for 7 and 14 d. Generally, positive results of ALP staining and ARS staining are observed in the Mg-4Zn, 0SrHA@Mg-4Zn, 5SrHA@Mg-4Zn and 10SrHA@Mg-4Zn groups. Besides, the group with higher Sr content exhibits more Ca nodulus and higher intensity of ALP staining.

3 Discussion

In the present study, Sr-doped HA coatings with different Sr contents were electrochemically deposited on Mg-4Zn substrates. From the SEM, EDS, TEM and SAED results presented in Fig.1, Table 1 and Fig.2, it is clear that the introduction of Sr into the HA coatings leads to significant change in the crystal distribution, lattice parameter and crystallinity. Sr ion shows an ionic radius of 0.113 nm, while, the radius of Ca ion is only 0.099 nm[16], so the Sr incorporation inevitably results in the larger d_{002} of the HA phase (see Fig. 2d), indicating larger lattice parameters. Furthermore, there are two inequivalent cation sites, i.e., Site I and Site II, in HA phase, and Sr induces more lattice distortion at Site II than Site I[17]. So the occupancy style of the substitutional ions can considerably affect the crystal formation. As stated by Terra et al.[18], when the atomic ratio of Sr/(Sr+Ca) is below 1%, a preference of Sr ion substitution is observed in Site I, while, Site II is progressively preferred at Sr concentration higher than 5 at%. In this work, the Sr/(Sr+Ca) in the two Sr-doped coatings are designed as 5 at% and 10 at% (in fact, 4.2 at% and 9.1 at%, respectively, see Table 1). The higher Sr content indicates more substitution at Site II, which leads to enhanced destabilization of crystal structure. Consequently, the SAED patterns show obvious decrease of crystallinity induced by Sr substitution (see Fig.2d). Besides, the smaller but more dense-packed crystal flakes on the Sr-doped coatings as shown in Fig.1 should be attributed to the restrained crystal growth, which also results from the severe lattice distortion.

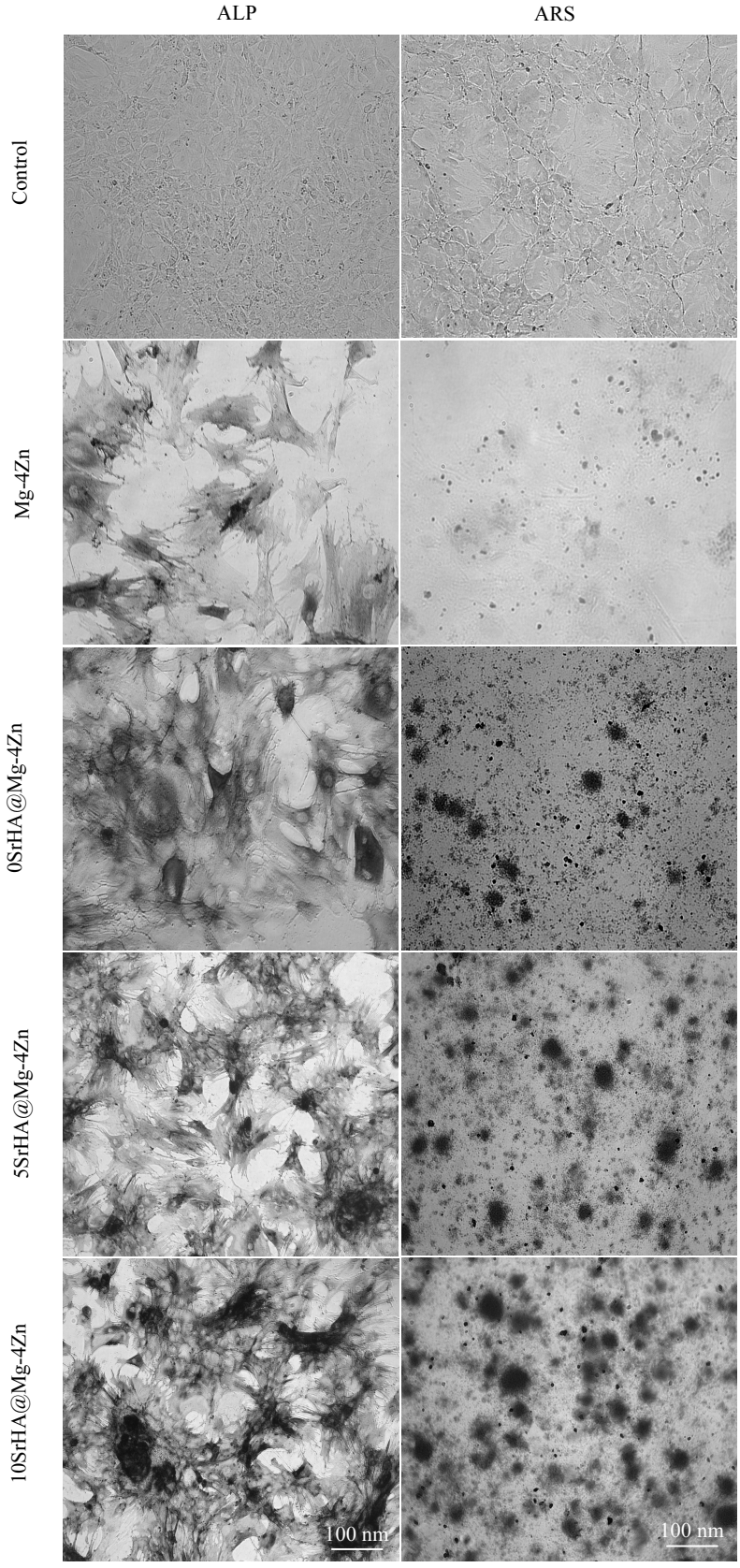

Fig. 9 ALP and ARS staining of the control regular medium group and the extraction mediums of the Mg-4Zn, 0SrHA@Mg-4Zn, 5SrHA@Mg-4Zn and 10SrHA@Mg-4Zn samples

From the biological point of view, the performances of implanted metallic biomaterials rely on the interaction mechanisms between the materials and surrounding tissues, so it is widely accepted that the surface physical properties, especially the topographical structure and hydrophilicity, are of prime importance in determining the cell responses[19]. As presented in Fig.3 and Table 2, the HA and Sr-doped HA coatings significantly increase the surface roughness compared to the bare Mg-4Zn alloy, and it seems that the incorporation of Sr leads to more peaks on the surfaces, which may result from the different HA crystal growth mechanisms. The wettability is an important parameter reflecting the surface energy of the biomaterials, and a hydrophilic surface is usually preferred for metallic biomaterials[20]. In this work, all the four samples show contact angles lower than 90°, but it is obvious that the HA coatings, especially the Sr-doped HA coatings, show much higher wettability as presented in Fig.4. Such a result is in agreement with the report[21] that when $R_a \geq 0.1$ μm the wettability is more mainly determined by the microscopic relief than by interfacial energetics.

The cytocompatibility of metallic biomaterials is not only determined by the physical properties, but also influenced by the surface chemistry[22, 23]. In this work, the surfaces of the as-prepared samples are Mg-4Zn, HA coating and Sr-doped coatings. The different composition leads to different ion release behaviors as presented in Fig.5. The Mg^{2+} release reflects the degradation of the Mg-based substrates, and the lower Mg^{2+} release amount of the coated samples demonstrates the corrosion resistant effects of the HA and Sr-doped HA coatings. The lowered corrosion rate of the Sr-incorporated groups may be due to the more dense-packed HA crystals. The release of Ca^{2+} and PO_4^{3-} corresponds to the degradation of HA phase. It is important to note that the Sr-incorporated HA coatings show similar Ca^{2+} and PO_4^{3-} evolution behavior, which does not agree with the release behavior on Ti substrates[24]. One possible explanation is that the degradation of Mg-based substrates results in alkaline environment around the surfaces, and thus influences the HA dissolution behavior.

Protein adsorption on the surface of biomaterials has been widely considered to be the first step after implantation, and the adsorbed proteins usually act as mediators between the materials and cells[25]. So it is necessary to evaluate the protein adsorption before performing cell viability assessments. The higher amount of protein adsorption on the 10SrHA coating (see Fig. 6) might be attributed to the smaller size of the HA crystal flakes, which can act as sites for preferential adsorption of BSA[10].

MSCs were selected for cytocompatibility tests in this work, because they are capable of self-replication and of differentiating into mesenchymal tissues, such as bone and cartilage[26]. The initial cell adhesion is critical to determine the final cell fate, and can be significantly influenced by protein adsorption, so the significantly improved cell adhesion on the Sr-doped HA coatings presented in Fig.7 is not unexpected. Similar to the cell adhesion results, the bare Mg-4Zn group shows the lowest cell viability, probably due to the strongest alkaline environment around the material surface. According to the ion release results after immersion for 72 h (see Fig.5), the main difference among the extract mediums of 0SrHA@Mg-4Zn, 5SrHA@Mg-4Zn and 10SrHA@Mg-4Zn is the Sr^{2+} concentrations. Since Sr incorporation in HA usually does not enhance cell proliferation[27], it is reasonable that the Sr-doped HA coated groups do not show a considerable difference when comparing with the HA coated groups as shown in Fig. 8. ALP is a marker for early osteogenic differentiation, and the calcium nodule formation is another marker reflecting the osteogenic differentiation in the late stage[28, 29]. The significantly increased ALP activity and more calcium nodule formation as shown in Fig.9 confirm the enhanced osteogenic differentiation induced by Sr, which is in accordance with the previous investigations[30, 31].

4 Conclusions

1) The substitution of Sr for Ca can increase the lattice parameters and decrease the crystallinity of the HA coatings.

2) The densely-packed crystal flakes on the Sr-doped samples act as barriers between the Mg-4Zn substrates and the SBF solution, leading to a better corrosion resistance with increasing Sr content. The presence of Sr in the coatings also results in a rougher surface and higher hydrophilicity, and therefore, the higher amount of protein adsorption and improved initial cell adhesion are not unexpected.

3) The introduction of Sr does not significantly change the cell proliferation on the HA coatings, but the ALP and ARS staining reveal that the osteogenic differentiation is induced by Sr.

4) These findings suggest that the incorporation of Sr can remarkably improve the corrosion resistance and osteointegration of the HA coated Mg-based biomaterials.

References

1 Zheng Y F, Gu X N, Witte F. *Materials Science and Engineering: R: Reports*[J], 2014, 77: 1

2 Yu H J, Wang J Q, Shi X T *et al*. *Advanced Functional Materials* [J], 2013: 4793

3 Zberg B, Uggowitzer P J, L Ffler J F. *Nature Materials* [J], 2009, 8: 887

4 Chen Y, Xu Z, Smith C *et al*. *Acta Biomaterialia*[J], 2014, 10: 4561

5 Zhu C, Lv Y, Qian C *et al*. *International Journal of Nanomedicine* [J], 2018, 13: 1881

6 Xin Y, Hu T, Chu P K. *Acta Biomaterialia*[J], 2011, 7: 1452

7 Hornberger H, Virtanen S, Boccaccini A R. *Acta Biomaterialia*

[J], 2012, 8: 2442
8 Jia Linan, Liang Chenghao, Huang Naibao *et al*. *Rare Metal Materials and Engineering* [J], 2015, 44(3): 592
9 Wen C, Guan S, Peng L *et al*. *Applied Surface Science* [J], 2009, 255: 6433
10 Zhou J, Li B, Han Y *et al*. *Nanomedicine*[J], 2016, 12: 1161
11 Liu W, Cheng M, Wahafu T *et al*. *Journal of Materials Science: Materials in Medicine*[J], 2015, 26: 203
12 Landi E, Tampieri A, Celotti G *et al*. *Acta Biomaterialia*[J], 2007, 3: 961
13 Xue W, Hosick H L, Bandyopadhyay A *et al*. *Surface and Coatings Technology* [J], 2007, 201: 4685
14 Zou Z, Chen J, Yan H *et al*. *Journal of Materials Engineering & Performance*[J], 2016, 25: 1974
15 Maegawa N, Kawamura K, Hirose M *et al*. *Journal of Tissue Engineering & Regenerative Medicine*[J], 2007, 1: 306
16 Li Z Y, Lam W M, Yang C *et al*. *Biomaterials*[J], 2007, 28: 1452
17 Boanini E, Gazzano M, Bigi A. *Acta Biomaterialia*[J], 2010, 6: 1882
18 Terra J, Dourado E R, Eon J G *et al*. *Physical Chemistry Chemical Physics*[J], 2009, 11: 568
19 Su Y, Luo C, Zhang Z *et al*. *Journal of the Mechanical Behavior of Biomedical Materials*[J], 2017, 77: 90
20 Hotchkiss K M, Reddy G B, Hyzy S L *et al*. *Acta Biomaterialia* [J], 2016, 31: 425
21 Rosales-leal J I, Rodr Guez-Valverde M A, Mazzaglia G *et al*. *Colloids & Surfaces A Physicochemical & Engineering Aspects* [J], 2010, 365: 222
22 Ponche A, Bigerelle M, Anselme K. *Proceedings of the Institution of Mechanical Engineers, Part H: Journal of Engineering in Medicine* [J], 2010, 224: 1471
23 Bagno A, Di Bello C. *Journal of Materials Science: Materials in Medicine* [J], 2004, 15: 935
24 Lindahl C, Pujari-palmer S, Hoess A *et al*. *Materials Science and Engineering: C* [J], 2015, 53: 322
25 Yang Y, Cavin R, Ong J L. *Journal of Biomedical Materials Research Part A* [J], 2003, 67A: 344
26 Wang X, Wang Y, Gou W *et al*. *International Orthopaedics*[J], 2013, 37: 2491
27 Ni G X, Yao Z P, Huang G T *et al*. *Journal of Materials Science: Materials in Medicine* [J], 2011, 22: 961
28 Liu Y T, Lee T M, Lui T S. *Colloids & Surfaces B Biointerfaces* [J], 2013, 106: 37
29 Gregory C A, Grady Gunn W, Peister A *et al*. *Analytical Biochemistry* [J], 2004, 329: 77
30 Schumacher M, Lode A, Helth A *et al*. *Acta Biomaterialia*[J], 2013, 9: 9547
31 Chung C J, Long H Y. *Acta Biomaterialia* [J], 2011, 7: 4081

Mg-4Zn 合金表面掺锶羟基磷灰石涂层：物理化学性质及体外细胞响应

石　伟[1]，赵大鹏[1]，尚　鹏[2]，聂和民[1]，张　远[1]，唐金成[1]

(1. 湖南大学，湖南 长沙 410082)

(2. 中国科学院深圳先进材料研究院，广东 深圳 518055)

摘　要：生物可降解镁合金由于具有高比强度、低弹性模量和优良生物相容性而受到广泛关注。然而，其过高的腐蚀速率却限制了其潜在的临床应用。因此，具有高生物相容性的羟基磷灰石（HA）涂层常被用于阻碍镁基体和周围生物环境的相互作用。采用电化学沉积法在 Mg-4Zn 合金表面制备了 HA 和掺锶（Sr）HA 涂层。利用扫描电子显微镜（SEM）、能谱（EDS）、透射电子显微镜（TEM）、三维激光扫描显微镜（3D LSM）和亲水角监测系统对材料表面性质进行表征。本研究还探讨了材料动态离子释放、蛋白吸附、细胞吸附、增殖与成骨分化行为。结果显示，HA 中引入 Sr 导致了晶格畸变和结晶度下降。涂覆掺 Sr HA 的样品中镁离子释放量比其他样品更低，说明耐腐蚀性更好。掺 Sr 样品表面蛋白吸附与初始细胞吸附的改善是由于其具有更高的表面粗糙度和亲水性。Sr 的引入并未显著改变细胞的增殖，却明显提高了成骨分化效果。综上所述，掺 Sr HA 涂层是一种非常有前景的镁合金保护性生物相容涂层。

关键词：掺锶羟基磷灰石；Mg-4Zn合金；动态离子释放；细胞活性；成骨分化

作者简介：石　伟，男，1989 年生，硕士生，湖南大学生物学院，湖南 长沙 410082，E-mail: ws@hnu.edu.cn